Intrinsic ferromagnetism with high Curie temperature and strong anisotropy in a ferroelastic VX monolayer (X = P, As)

Xuli Cheng,[1] Shaowen Xu,[1] Fanhao Jia ●,[1,*] Guodong Zhao ●,[1,2] Minglang Hu,[1] Wei Wu,[1] and Wei Ren[1,†]

[1]*Physics Department, Shanghai Key Laboratory of High Temperature Superconductors, State Key Laboratory of Advanced Special Steel, International Centre of Quantum and Molecular Structures, Shanghai University, Shanghai 200444, China*

[2]*School of Microelectronics, Fudan University, Shanghai 200433, China*

Two-dimensional (2D) multiferroic materials, with combined large magnetic anisotropic energy (MAE) and high Curie temperature (T_C), have great potential in emerging electronic device applications, such as high-density multistate data storage and fast operation. However, various 2D spintronic materials fabricated in experiment, so far have small MAE and low T_C. Using first-principles calculations, we proposed two VX (X = P, As) monolayers, which are identified to possess robust stability dynamically, thermally, and mechanically. VX monolayers are half-metals with coexisting ferroelastic and ferromagnetic properties. Moreover, their ground states exhibit significant in-plane MAEs of 101.48 and 262.68 μeV per V atom for VP and VAs monolayers, respectively. Additionality, the Curie temperatures of VP and VAs monolayers predicted from Heisenberg model are as high as 545 and 890 K, respectively, and the ferromagnetism could survive at room temperature. Our results are beneficial for further research on 2D multiferroics and provide the possibility for future nanodevices.

DOI: 10.1103/PhysRevB.104.104417

I. INTRODUCTION

Two-dimensional (2D) multiferroic materials, possessing more than two ferroic properties [1–3], have attracted much attention owing to their rich applications in emerging nanoelectronics [4–7]. Generally, the focus of 2D multiferroics has been on the simultaneous ferromagnetic (FM) and ferroelectric (FE) orders [8,9], leaving the materials with the ferroelasticity and ferromagnetism less reported in the literature. As far as we know, magnetically doped 2D materials with the room temperature T_C might have been successfully realized in laboratory, such as Cr-doped ZnTe at 300 ± 10 K [10–13] and Mn-doped GaN at 300 K [14,15]. However, the conventional doping of transition metals meets many challenges to make a breakthrough in experiments, for example, one of the problems is the low solubility [16]. Furthermore, a small magnetic anisotropic energy (MAE) hardly counteracts the thermal fluctuations, which also limits the development of 2D FM materials. Fortunately, a series of new 2D FM materials have been predicted, for instance MnP and CrP monolayers with T_C up to 495 K (232 K) and MAE up to 166 μeV per Mn (217 μeV per Cr), respectively [17,18]. On the other hand, among various ferroic properties, ferroelasticity shows good compatibility with other orders [19]. Although several 2D materials of ferroelastic (FA) and FM multiferroics have been proposed to date, including MnNX (X = halogen element) [5], VSSe [20], α-SnO [21], and CrSX (X = halogen element) monolayers [22], quite few could sustain stable ferromagnetism at room temperature [5,20]. For the applications of high-performance spintronic devices, finding 2D multiferroics

simultaneously possessing FM and FA orderings with large spin-orbit coupling (SOC) and high T_C is of great importance.

The VP monolayer has been investigated in theory recently [23], by studying the optical, electronic transport, different substrates effects, and H_2O molecule adsorption. In this work, we focus on the 2D multiferroic properties in VP and VAs monolayers. They are found to be both half-metals with high T_C and strong MAE. The T_C of VP and VAs monolayers from Heisenberg model are 545 and 890 K, respectively. The MAEs are as large as 101.48 μeV/V for VP monolayer and 262.68 μeV/V for VAs monolayer, respectively. Moreover, we also study the ferroelasticity properties, and find the reversible strain is 0.11% for VP monolayer and 1.52% for VAs monolayer. Our discovery provides an ideal platform for exploring 2D multiferroic materials, and the excellent performances of VP and VAs monolayers show great potential in spintronics applications.

II. COMPUTATIONAL METHOD

Our first-principles density functional theory (DFT) calculations are carried out with the generalized gradient approximation proposed by Perdew, Burke, and Ernzerhof (PBE) [24], which is implemented in the Vienna *ab initio* simulation package (VASP) [25]. We take the energy cutoff as 600 eV and consider an additional effective Hubbard U_{eff} = 4.0 eV for V to reduce the delocalization error of d electrons [26,27]. The Γ centered k grids are adopted to be 8 × 8 × 1. The atomic positions are fully relaxed until the maximum force on each atom was less than 10^{-3} eV/Å. To solve the underestimating band gap problem of PBE, the screened hybrid functional HSE06 [28] is applied to calculate the more accurate electronic structures. The van der Waals (vdW) correction is included by using the optB86b-vdW method. Here, we adopt the vacuum layer more than 30 Å to avoid the
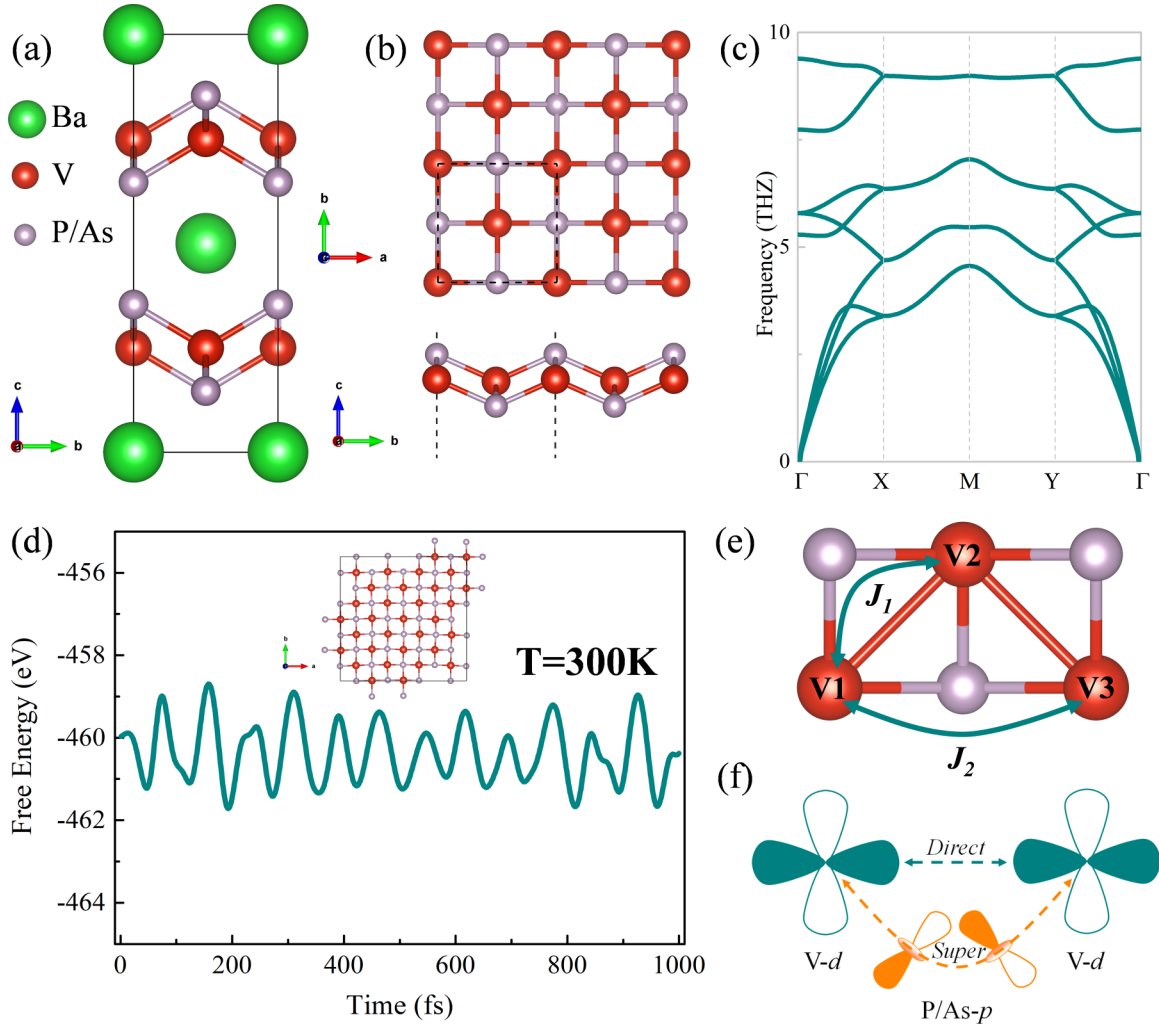
FIG. 1. (a) Crystal structure of layered ternary compounds BaV_2X_2 ($X = P$, As). (b) The top and side views of the VP monolayer. The dashed rectangle indicates the primitive cell. (c) The phonon spectra of the VP monolayer. (d) The evolution of energy over time at $T = 300\,K$ from molecular dynamics simulations of VP monolayer. (e) The exchange constants J_1 and J_2 are the NN and NNN interaction parameters, respectively. (f) Illustration of the direct-exchange and superexchange mechanisms.

interaction between periodic images. The SOC is also taken into account in our MAE calculations. The phonon dispersion is calculated by density-functional perturbation theory as implemented in the PHONOPY package [29,30].

III. RESULTS AND DISCUSSION

A. Geometric structures and stabilities

Bulk BaV_2X_2 ($X = P$, As) crystals belonging to the *Immm* space group have been predicted as a class of layered FM half-metallic materials [17,31] with alternating VX and Ba layer along the [001] direction. Their crystal and electronic structures are shown in Fig. 1(a) and Fig. S1 (see Supplemental Material (SM) [32]), respectively. Due to van der Waals interaction, VX monolayers are thought to be possibly exfoliated from their bulk counterpart. The cleavage energy (E_{cl}) is calculated as $0.105\,eV\,Å^{-2}$ for VP monolayer ($0.101\,eV\,Å^{-2}$ for VAs monolayer), comparable to the MXenes systems ($0.086\,eV - 0.205\,eV\,Å^{-2}$) [33–35]. To demonstrate the stability of VX monolayers in Fig. 1(b), the phonon spectra,

elastic constant calculations, and *ab initio* molecular dynamics simulations are performed. As shown in Fig. 1(c), we find that there is no obvious imaginary mode in the whole Brillouin zone, which confirms the dynamic stability of the VX monolayers. Additionally, the corresponding fluctuations of total energies and the final structure configuration for 1000 fs at 300 K are plotted in Fig. 1(d), where the geometries are still maintained without broken bond or phase transition, showing the good thermal stability of the VX monolayers (see also Fig. S2 for VAs monolayer). Furthermore, according to the elastic constants listed in Table S1, they also satisfy the Born mechanical stability criteria: $C_{11} > |C_{12}| > 0$ and $C_{66} > 0$. The optimized structures of VX monolayers are displayed in Fig. 1(b) for the top and side views. Its crystal structure with a 2D rectangle lattice belongs to the point group *mmm*, while stacked in 3D has a space group of P*mnm*. The lattice parameters of VP monolayer are calculated to be $a = 4.427\,Å$, $b = 4.422\,Å$ for VP monolayer ($a = 4.437\,Å$, $b = 4.504\,Å$ for VAs monolayer) at the vdW-DF-optB86b+U level ($U = 4\,eV$).
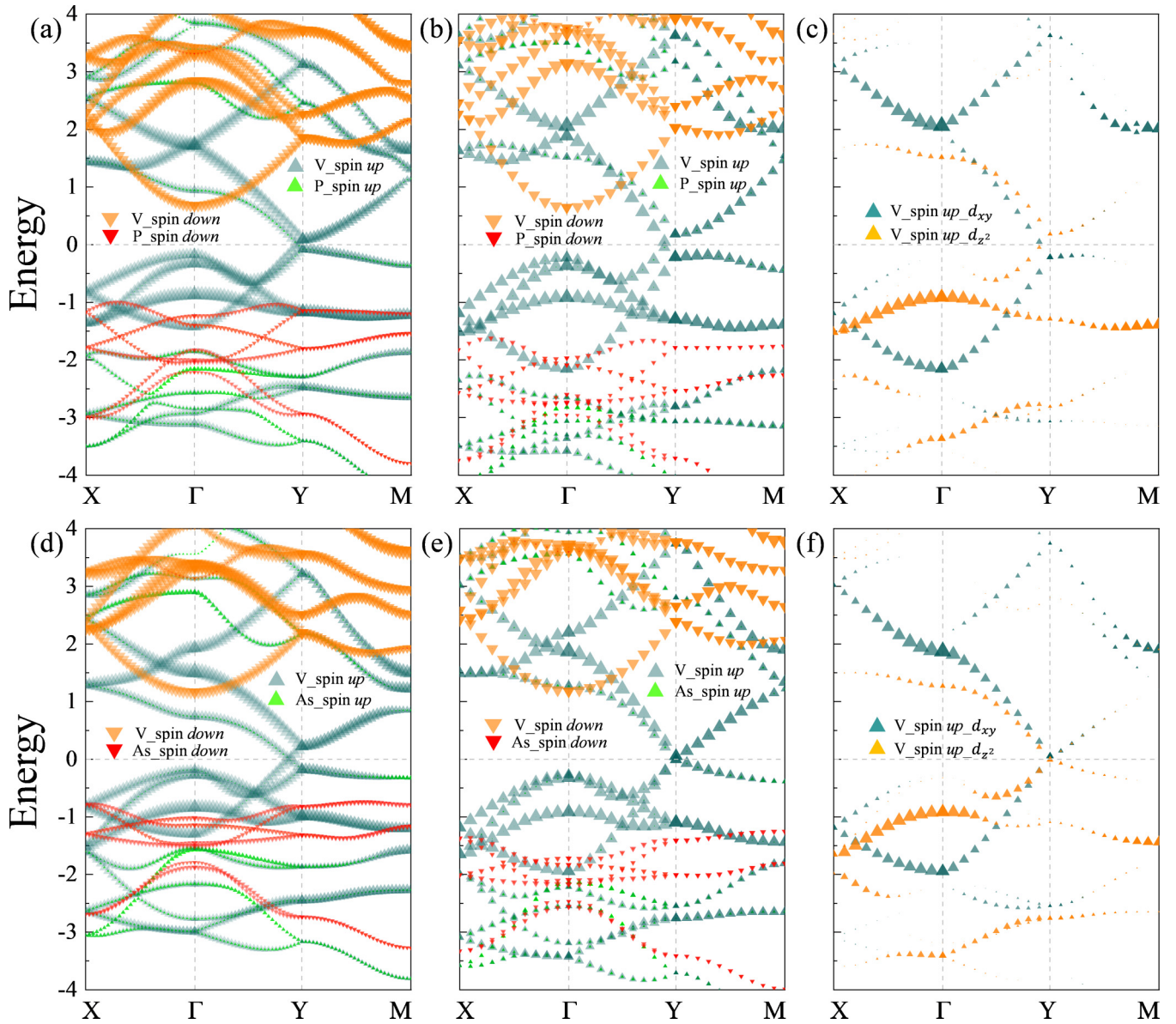
FIG. 2. The projected electronic energy band structures of (a) VP and (d) VAs monolayers calculated by using vdW-DF-optB86b+U method. The HSE06 band structures are shown in (b) VP and (e) VAs, with (c) and (f) highlighting two most-contributing channels near the Fermi levels in (b) and (e), respectively.

B. Electronic properties

Due to the existence of d orbitals in VX monolayers, the PBE method might be unable to describe the electronic properties adequately. Therefore, vdW-DF-optB86b+U and hybrid functionals (HSE06) are considered here. The spin-polarized band structures from the vdW-DF-optB86b+U method are shown in Figs. 2(a) and 2(d). The conduction band minima of the VP and VAs monolayers are mainly contributed by V d_{xy} orbitals, while the valence band maxima are mainly contributed by V d_{z^2} orbital shown in Figs. 2(c) and 2(f). More importantly, the spin-up bands cross the Fermi level while the spin-down bands are far away from Fermi level, leaving a large spin-down band gap of 1.6793 eV for VP monolayer (1.9018 eV for VAs monolayer). It suggests that the VX monolayers are intrinsically half-metallic and further

confirmed by the more accurate HSE06 method as shown in Figs. 2(b) and 2(e). The spin-down bands are also farther away from the Fermi level, leading significant band gaps (2.2721 eV for VP monolayer, 2.4310 eV for VAs monolayer), large enough to prevent the thermally excited spin-flip transition and maintains the half-metallicity at room temperature. This interesting finding provides a new possibility for design of spin-filter and spin-separator [36,37] and makes VP and VAs monolayers become useful in the application of 2D spintronics.

C. Magnetic properties

To determine the magnetic ground state, the $2 \times 2 \times 1$ supercells of the VX monolayers with four magnetic
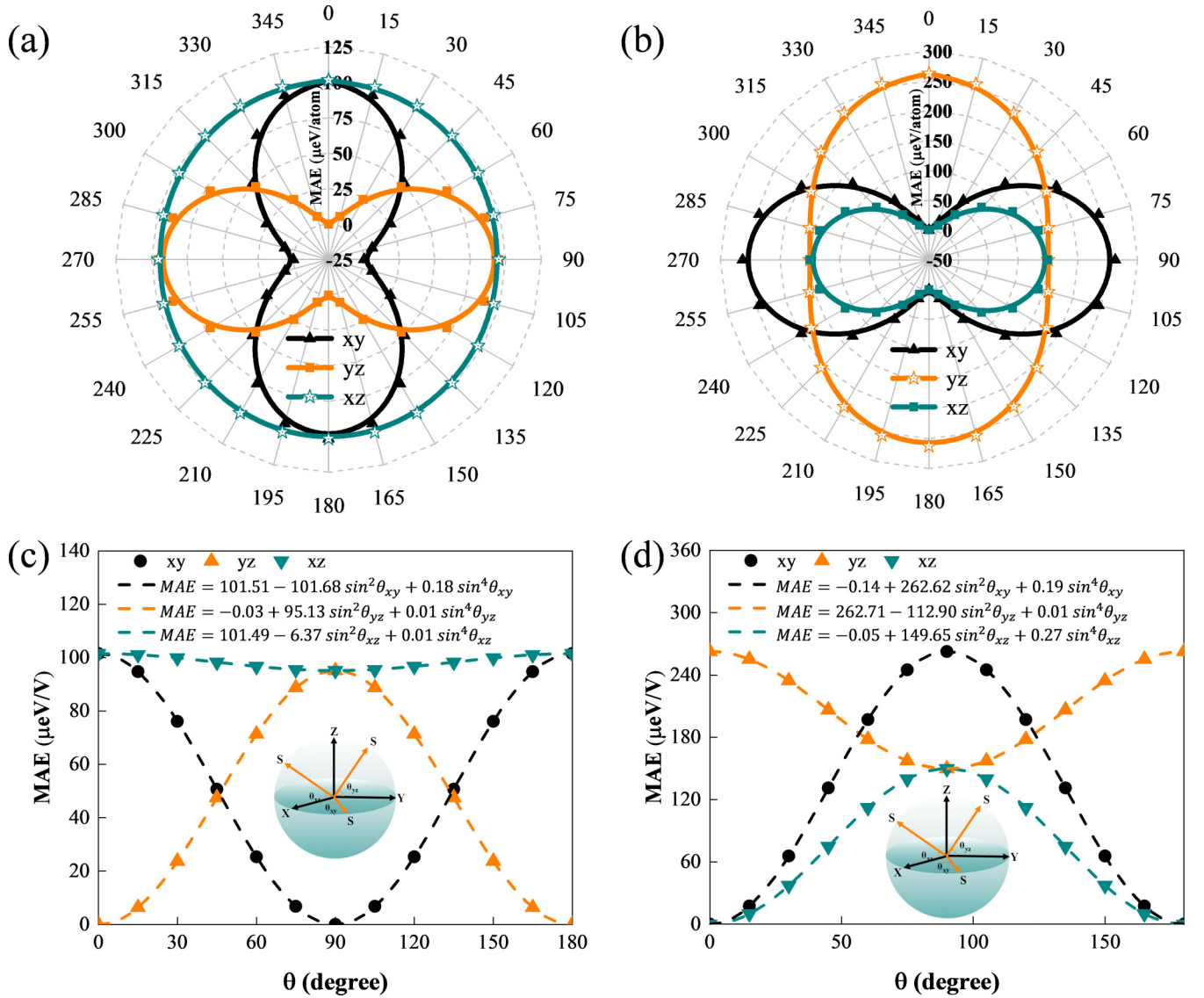
FIG. 3. Angular dependences of the MAEs in the polar and Cartesian coordinate systems for (a), (c) VP monolayer and (b), (d) VAs monolayer with the direction of magnetization lying on three different planes. The inset illustrates that the spin vector S on the xy, yz, and xz planes is rotated with an angle θ about the x, y, and z axes, respectively, $\theta_{xz} = 0°$ represents the moment lying in the z axis.

configurations are constructed, as shown in Fig. S3. The energy differences between the antiferromagnetic (AFM) states and the FM ground state are shown in Table S2. It is found that VP and VAs monolayers both maintain FM ground states, and the FM state is robust against the external strain, electric field, and doping. From the spin density results (Fig. S4), one can find the spin magnetic moments are mainly contributed by an unpaired electron of the V^{3+} ions. The magnetic moments of VP and VAs are 2.17 and 2.23 μ_B per V atom from our DFT calculations. It can be well understood by analyzing the valence electron configuration of V atom ($3d^3 4s^2$), which becomes V^{3+} ($3d^2$ configuration) after transferring $3e^-$ to P or As atom. Unpaired $2e^-$ electrons prefer to have high spin alignment with $2\mu_B$ based on Hund rules [38,39] and the Pauli exclusion principle, in very good agreement with our DFT calculations.

The microscopic mechanism of FM ground state for VX monolayers is explained by exchange interaction between two adjacent spin magnetic moments, including the nearest-neighbor (NN) exchange (J_1) and the next nearest-neighbor (NNN) exchange (J_2). As shown in Figs. 1(e) and 1(f), it is found that the V_1-V_2 distance (3.13 Å) is so large that the direct magnetic exchange interaction between them is relatively weak. The superexchange interaction between magnetic atoms (V_1, V_3) with d orbitals linked by a nonmagnetic P/As atom is stronger. According to the Heitler-London model [40], the exchange integral J can be written as $J \approx 2k + 4\beta S$, where k is the potential exchange, β is the hopping integral and S is the overlap integral, respectively. According to the Goodenough-Kanamori-Anderson rules [41–44], the bond-angle of V_1-P/As-V_2 of 77.6° (J_1) and V_1-P/As-V_3 of 123.8° (J_2) are close to 90°, which indicates the overlap integral S

TABLE I. The magnetic coupling parameters J_1, J_2, and J_3 (meV), magnetic anisotropy energies (μeV per V) in different directions, T_C(K) from Ising and anisotropic Heisenberg (AH) models for VX (X = P, As) monolayers, and the magnetic moment M (μ_B) per V atom.

System	J_1	J_2	J_3	E (100)	E (010)	E (001)	$T_{C\text{-Ising}}$	$T_{C\text{-AH}}$	M
VP	26.30	10.41	−2.21	101.48	0	95.14	1850	545	2.17
VAs	28.87	3.55	12.40	0	262.68	149.82	2840	890	2.23

approaching zero. Thus, J is reduced to $2k$. Since the Hund rule requires the electrons in the p orbitals of P/As atom to be arranged parallel, meanwhile, the spins of the magnetic atom V are parallel, leading to a positive k. As a result, VP and VAs monolayers are favored to have FM ground state with J_1 and J_2 both having positive signs.

The MAE [45] derived from the SOC plays a crucial role in the spintronics and long-range FM ordered 2D materials. Based on the uniaxial tetragonal symmetry model (Fig. 3), we compared the MAEs of VP and VAs monolayers in the xy, yz, xz planes as function of the magnetization angle θ. The angle-dependent MAE in the polar coordinate system and Cartesian coordinate system are shown in Figs. 3(a) and 3(b) and Figs. 3(c) and 3(d) respectively. The angular dependence of MAE in Cartesian coordinate system can be fitted by [46]

$$\text{MAE}(\theta) = E_0 + K_1 \sin^2\theta + K_2 \sin^4\theta, \quad (1)$$

where E_0 is a constant energy shift, K_1 and K_2 are, respectively, the quadratic and quartic contributions to the energy and θ is the azimuthal angle of rotation. By comparing the energy difference of the three planes, we find that the magnetic easy axes of the VP and VAs monolayers both prefer the in-plane direction. In detail, both VP and VAs monolayers align the moments along the short axis. Besides, VP and VAs monolayers exhibit strong magnetic anisotropy, namely 101.48 μeV per V atom for VP and 262.68 μeV per V atom for VAs. The large MAEs should be sufficient to stabilize FM ordering against the thermal fluctuation at higher temperature.

To predict the T_C of VP and VAs monolayers, Monte Carlo (MC) simulations based on the Ising and Heisenberg models were performed. Here, we considered the NN, the NNN and the third nearest-neighbor (TNN) exchange interactions. The Hamiltonian of Heisenberg model is defined as [47,48]

$$H = -2J_1 \sum_{\langle i,j \rangle} S_i \cdot S_j - 2J_2 \sum_{\langle\langle i,j \rangle\rangle} S_i \cdot S_j - 2J_3$$
$$\times \sum_{\langle\langle\langle i,j \rangle\rangle\rangle} S_i \cdot S_j - D \sum_i \left| S_i^e \right|^2, \quad (2)$$

where $\langle i, j \rangle$, $\langle\langle i, j \rangle\rangle$ and $\langle\langle\langle i, j \rangle\rangle\rangle$ denote the NN, NNN, and TNN spins. $J_{1,2,3}$ are the Heisenberg exchange constants between the NN, NNN, and TNN spins, respectively. S is the spin vector of V atom; S_i^e is the spin component along the easy magnetic axis and D is the uniaxial anisotropy of each magnetic ion. Supercells ($2 \times 2 \times 1$) were chosen to perform MC simulations, which contain 16 magnetic moments. We construct four magnetic configurations (Fig. S3) to compute J_1, J_2, and J_3, since the lengths of the lattice constants a and b

are not much different, J_2 in the a/b direction can be regarded as isotropic, with the following equations:

$$\frac{E_{\text{FM}}}{8} = -E_0 - (4J_1 + 4J_2 + 4J_3)|S|^2 - D|S|^2, \quad (3)$$

$$\frac{E_{\text{AFM1}}}{8} = -E_0 - (-4J_1 + 4J_2 + 4J_3)|S|^2 - D|S|^2, \quad (4)$$

$$\frac{E_{\text{AFM2}}}{8} = -E_0 - (-4J_3)|S|^2 - D|S|^2, \quad (5)$$

$$\frac{E_{\text{AFM3}}}{8} = -E_0 - (-4J_2 + 4J_3)|S|^2 - D|S|^2. \quad (6)$$

Thus,

$$J_1 = \frac{E_{\text{AFM1}} - E_{\text{FM}}}{64}, \quad (7)$$

$$J_2 = \frac{J_1}{2} + \frac{E_{\text{AFM3}} - E_{\text{AFM1}}}{64}, \quad (8)$$

$$J_3 = \frac{J_2}{2} + \frac{E_{\text{AFM2}} - E_{\text{AFM3}}}{64}. \quad (9)$$

We obtain the J_1, J_2, and J_3 of VP monolayer to be 26.30, 10.41, and −2.21 meV (28.87, 3.55, and 12.40 meV for VAs) as shown in Table I, respectively. The uniaxial anisotropy energy parameter D obtained by using the magnetic anisotropy energies is [48]:

$$D = \frac{E_{\text{max}}(\text{axis}) - E_{\text{easy}}(\text{axis})}{|S|^2}. \quad (10)$$

The values are found to be 101.48 μeV and 262.68 μeV for VP and VAs monolayers, respectively. The specific heat capacity (C_v) versus temperature of VP and VAs monolayers (Fig. 4) suggests that the T_C of VP is as high as 545 K, and 890 K for VAs. These critical values are higher than most reported 2D magnetic materials. We have also estimated T_C based on the Ising model (Fig. S5), giving the significantly overestimated T_C results much higher than the more reasonable values from Heisenberg model [49].

D. Ferroelastic properties

Based on the unique geometric structures of the VP and VAs monolayers, ferroelastic properties are discussed here. The two energy-equivalent ground states, the initial state (IS) and the final state (FS), could be transformed to each other. The climbing-image nudged elastic band method is used to calculate the energy barrier. As shown in Fig. 5 and Fig. S6, IS and FS are connected by a transition state (TS) with equal lattice constants $|a| = |b|$. The overall transition barriers of VP and VAs monolayers are 1.209×10^{-2} and 2.623 meV per V,
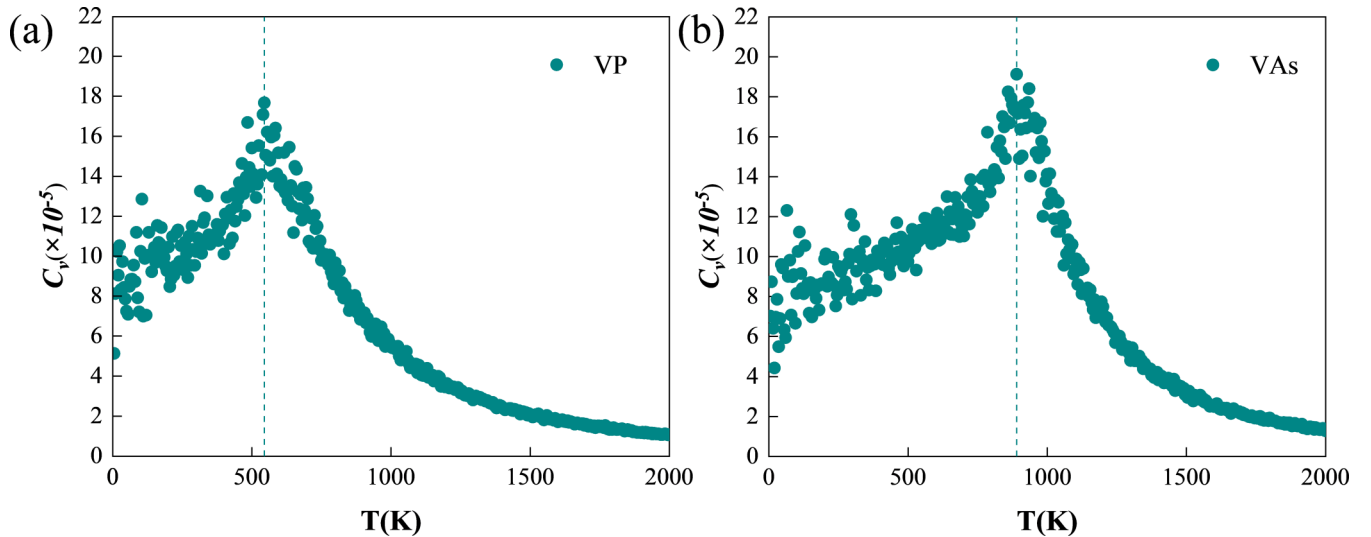
FIG. 4. The Monte Carlo simulated specific heat C_v as a function of temperature using the Heisenberg model for (a) VP monolayer and (b) VAs monolayer.

while the calculation of transformation strain matrix suggests that there is a 0.09% tensile strain (0.45% compressive strain) along the a/b axis and a 0.14% compressive strain (1.07% tensile strain) along the b/a axis for the IS/FS. The values of VP monolayer are very small, but meanwhile it shows a much lower transition barrier than that in VAs monolayer. Another important factor affecting the ferroelastic performance is the reversible strain defined as $(b/a - 1) \times 100\%$. It is calculated to be 0.11% for VP monolayer and 1.52% for VAs monolayer, which are comparable to most ferroelastic materials [5,50,51]. Such low switching barrier and moderate reversible strain both suggest the VAs monolayer would exhibit strong switching signal and high experimental feasibility. Moreover, the conversion of IS to FS is always accompanied by a 90°

rotation of the magnetic easy axis, which makes it possible to adjust the spin direction *via* strain as well. Such a feature is expected to provide new possibilities for the design of controllable spintronic devices.

IV. CONCLUSIONS

In summary, based on first-principles calculations, we reveal two stable 2D multiferroic materials VP and VAs monolayers with coexisting ferromagnetism and ferroelasticity. Both systems show dynamic, thermal, and mechanical stability and they can easily be fabricated from peeling the bulk thanks to the low exfoliation energies. Furthermore, VP and VAs monolayers have high Curie temperatures (545 K for VP and 890 K for VAs) and large MAE (101.48 μeV/V atom for VP and 262.68 μeV/V atom for VAs). Our discovery provides an ideal platform for exploring 2D multiferroic materials and spintronic devices in practical applications.

FIG. 5. The energy barrier for ferroelastic switching of VAs monolayer. The insets are schematic diagrams of the initial state (IS), transition state (TS) and final state (FS).

[1] K. Yamauchi and S. Picozzi, Phys. Rev. Lett. **105**, 107202 (2010).

[2] S. Xu, F. Jia, X. Cheng, and W. Ren, arXiv:2105.14757 (2021).

[3] S. Xu, F. Jia, G. Zhao, W. Wu, and W. Ren, J. Mater. Chem. C **9**, 9130 (2021).

[4] F. Jia, S. Xu, G. Zhao, C. Liu, and W. Ren, Phys. Rev. B **101**, 144106 (2020).

[5] M. Hu, S. Xu, C. Liu, G. Zhao, J. Yu, and W. Ren, Nanoscale **12**, 24237 (2020).

[6] J.-J. Zhang, L. Lin, Y. Zhang, M. Wu, B. I. Yakobson, and S. Dong, J. Am. Chem. Soc. **140**, 9768 (2018).

[7] W. Luo, K. Xu, and H. Xiang, Phys. Rev. B **96**, 235415 (2017).

[8] C. Huang, Y. Du, H. Wu, H. Xiang, K. Deng, and E. Kan, Phys. Rev. Lett. **120**, 147601 (2018).

[9] Y. Lai, Z. Song, Y. Wan, M. Xue, C. Wang, Y. Ye, L. Dai, Z. Zhang, W. Yang, H. Du, and J. Yang, Nanoscale **11**, 5163 (2019).

[10] L. Zhao, B. Zhang, Q. Pang, S. Yang, X. Zhang, W. Ge, and J. Wang, Appl. Phys. Lett. **89**, 092111 (2006).

[11] D. Soundararajan, D. Mangalaraj, D. Nataraj, L. Dorosinskii, and K. H. Kim, Mater. Lett. **87**, 113 (2012).

[12] H. Saito, V. Zayets, S. Yamagata, and K. Ando, Phys. Rev. Lett. **90**, 207202 (2003).

[13] H. Saito, V. Zayets, S. Yamagata, and K. Ando, J. Appl. Phys. **93**, 6796 (2003).

[14] H. J. Choi, H. K. Seong, J. Chang, K. I. Lee, Y. J. Park, J. J. Kim, S. K. Lee, R. He, T. Kuykendall, and P. Yang, Adv. Mater. **17**, 1351 (2005).

[15] K. Ando, Appl. Phys. Lett. **82**, 100 (2003).

[16] M. Kan, J. Zhou, Q. Sun, Y. Kawazoe, and P. Jena, J. Phys. Chem. Lett. **4**, 3382 (2013).

[17] B. Wang, Y. Zhang, L. Ma, Q. Wu, Y. Guo, X. Zhang, and J. Wang, Nanoscale **11**, 4204 (2019).

[18] A.-N. Ma, P.-J. Wang, and C.-W. Zhang, Nanoscale **12**, 5464 (2020).

[19] N. A. Spaldin, S.-W. Cheong, and R. Ramesh, Phys. Today **63**(10), 38 (2010).

[20] C. Zhang, Y. Nie, S. Sanvito, and A. Du, Nano Lett. **19**, 1366 (2019).

[21] L. Seixas, A. S. Rodin, A. Carvalho, and A. H. Castro Neto, Phys. Rev. Lett. **116**, 206803 (2016).

[22] B. Xu, S. Li, K. Jiang, J. Yin, Z. Liu, Y. Cheng, and W. Zhong, Appl. Phys. Lett. **116**, 052403 (2020).

[23] Y. Kadioglu, Mater. Sci. Eng. B **268**, 115111 (2021).

[24] J. P. Perdew, K. Burke, and M. Ernzerhof, Phys. Rev. Lett. **77**, 3865 (1996).

[25] G. Kresse and J. Furthmüller, Phys. Rev. B **54**, 11169 (1996).

[26] X. Gao, R. Lian, L. He, Q. Fu, S. Indris, B. Schwarz, X. Wang, G. Chen, H. Ehrenberg, and Y. Wei, J. Mater. Chem. A **8**, 17477 (2020).

[27] D. Dey, T. Maitra, and A. Taraphder, AIP Conf. Proc. **1832**, 090021 (2017).

[28] J. Heyd, G. E. Scuseria, and M. Ernzerhof, J. Chem. Phys. **118**, 8207 (2003).

[29] A. Togo, F. Oba, and I. Tanaka, Phys. Rev. B **78**, 134106 (2008).

[30] A. Togo and I. Tanaka, Scr. Mater. **108**, 1 (2015).

[31] J. Zeng, S. Qin, C. Le, and J. Hu, Phys. Rev. B **96**, 174506 (2017).

[32] See Supplemental Material at http://link.aps.org/supplemental/10.1103/PhysRevB.104.104417 for further details, which includes the lattice constants and elastic constants of the VX (X = P, As) monolayers, schematic diagrams of different magnetic configurations and relative energy, and the Monte Carlo simulated specific heat Cv as a function of temperature using the Ising mode. The electronic structure information of the bulk BaV_2X_2 (X = P, As).

[33] L. Hu, X. Wu, and J. Yang, Nanoscale **8**, 12939 (2016).

[34] J. He, P. Lyu, and P. Nachtigall, J. Mater. Chem. C **4**, 11143 (2016).

[35] G. Gao, G. Ding, J. Li, K. Yao, M. Wu, and M. Qian, Nanoscale **8**, 8986 (2016).

[36] W.-F. Tsai, C.-Y. Huang, T.-R. Chang, H. Lin, H.-T. Jeng, and A. Bansil, Nat. Commun. **4**, 1500 (2013).

[37] R. Soulen, J. Byers, M. Osofsky, B. Nadgorny, T. Ambrose, S. Cheng, P. R. Broussard, C. Tanaka, J. Nowak, and J. Moodera, Science **282**, 85 (1998).

[38] J. Katriel and R. Pauncz, in *Advances in Quantum Chemistry* (Elsevier, Amsterdam, 1977), p. 143.

[39] L. de'Medici, J. Mravlje, and A. Georges, Phys. Rev. Lett. **107**, 256401 (2011).

[40] J.-P. Launay and M. Verdaguer, *Electrons in Molecules: From Basic Principles to Molecular Electronics* (Oxford University Press, Oxford, 2014).

[41] S. Wolf, D. Awschalom, R. Buhrman, J. Daughton, v. S. von Molnár, M. Roukes, A. Y. Chtchelkanova, and D. Treger, Science **294**, 1488 (2001).

[42] P. W. Anderson, Phys. Rev. **115**, 2 (1959).

[43] J. B. Goodenough, Phys. Rev. **100**, 564 (1955).

[44] R. Janisch and N. A. Spaldin, Phys. Rev. B **73**, 035201 (2006).

[45] M. Darby and E. Isaac, IEEE Trans. Magn. **10**, 259 (1974).

[46] K. H. J. Buschow and F. R. Boer, *Physics of Magnetism and Magnetic Materials* (Springer, Berlin, 2003), Vol. 7.

[47] G.-D. Zhao, X. Liu, T. Hu, F. Jia, Y. Cui, W. Wu, M.-H. Whangbo, and W. Ren, Phys. Rev. B **103**, 014438 (2021).

[48] S. Wang, J. Wang, and M. Khazaei, Phys. Chem. Chem. Phys. **22**, 11731 (2020).

[49] A. Kabiraj, M. Kumar, and S. Mahapatra, npj Comput. Mater. **6**, 35 (2020).

[50] M. Wu and X. C. Zeng, Nano Lett. **16**, 3236 (2016).

[51] X. Xu, Y. Ma, T. Zhang, C. Lei, B. Huang, and Y. Dai, Nanoscale Horiz. **5**, 1386 (2020).